Synergetic Chemical Coupling Controls the Uniformity of Carbon Nanotube Microstructure Growth

Mostafa Bedewy,[†,‡,⊥] Brittan Farmer,[†,§,⊥] and A. John Hart[†,‡,*]

[†]Mechanosynthesis Group, Department of Mechanical Engineering, University of Michigan, 2350 Hayward Street, Ann Arbor, Michigan 48109, United States, [‡]Mechanosynthesis Group, Department of Mechanical Engineering and Laboratory for Manufacturing and Productivity, Massachusetts Institute of Technology, 77 Massachusetts Avenue, Cambridge, Massachusetts 02139, United States, and [§]Department of Mathematics, University of Michigan, 530 Church Street, Ann Arbor, Michigan 48109, United States. [⊥]M. Bedewy and B. Farmer contributed equally.

ABSTRACT Control of the uniformity of vertically aligned carbon nanotube structures (CNT "forests"), in terms of both geometry and nanoscale morphology (density, diameter, and alignment), is crucial for applications. Many studies report complex and sometimes unexplained spatial variations of the height of macroscopic CNT forests, as well as variations among micropillars grown from lithographically patterned catalyst arrays. We present a model for chemically coupled CNT growth, which describes the origins of synergetic growth effects among CNT micropillars in proximity. *Via* this model, we propose that growth of CNTs is locally enhanced by active species that are catalytically produced at the substrate-bound nanoparticles. The local concentration of these active species modulates the growth rate of CNTs, in a spatially dependent manner driven by diffusion and local generation/consumption at the catalyst sites. Through experiments and numerical simulations, we study how the uniformity of CNT micropillars can be influenced by their size and spacing within arrays and predict the widely observed abrupt transition between tangled and vertical CNT growth by assigning a threshold concentration of active species. This mathematical framework enables predictive modeling of spatially dependent CNT growth, as well as design of catalyst patterns to achieve engineered uniformity.

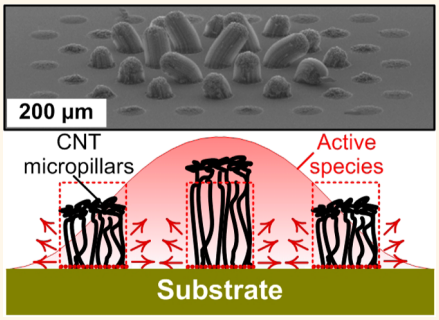

KEYWORDS: chemical vapor deposition · carbon nanotubes · microstructure · diffusion · reaction

Beyond the properties of individual carbon nanotubes (CNTs) and the applications of bulk CNT powders,[1] a new frontier of applications is potentially accessible by harnessing the properties of large numbers of CNTs in organized assemblies. In academic research, vertically aligned CNT "forests" have been incorporated into different material systems including thin films, interface layers, and structured 3D geometries such as micropillars or coatings on woven fibers. The individual CNT properties as well as the hierarchical morphology of CNT forests gives rise to novel and widely tunable mechanical behavior,[2,3] as well as electrical transport[4,5] and thermal transport properties that can be related to the CNT alignment and contact behavior.[6,7] Nevertheless, uniformity in the geometry, density, and diameter of the CNTs within the forest is needed to effectively engineer its functional properties.

In several published reports as well as in our own previous work, it is apparent that typical chemical vapor deposition (CVD) growth conditions for CNT forests create significant spatial nonuniformities. These include geometric nonuniformities (*i.e.*, sloped heights) of macroscopic CNT forests,[8,9] as well as microscopic CNT pillars.[10−12]

A typical CNT micropillar array from our work exemplifies these variations. Micropillars grown to high aspect ratios (30 min growth time, Figure 1a) strikingly curve outward along the periphery of the array. Micropillars with much lower aspect ratio (3 min growth time, Figure 1b, c, d) are shorter toward the edges and corner of the array, and the corner catalyst pattern feature does not yield a CNT forest. In addition, the micropillars near the corner of the array do not completely cover the catalyst pattern and have crowned top surfaces. Moreover, we frequently observe that the growth of

* Address correspondence to ajhart@mit.edu.

Received for review February 4, 2014 and accepted May 3, 2014.

Published online May 03, 2014
10.1021/nn500698z

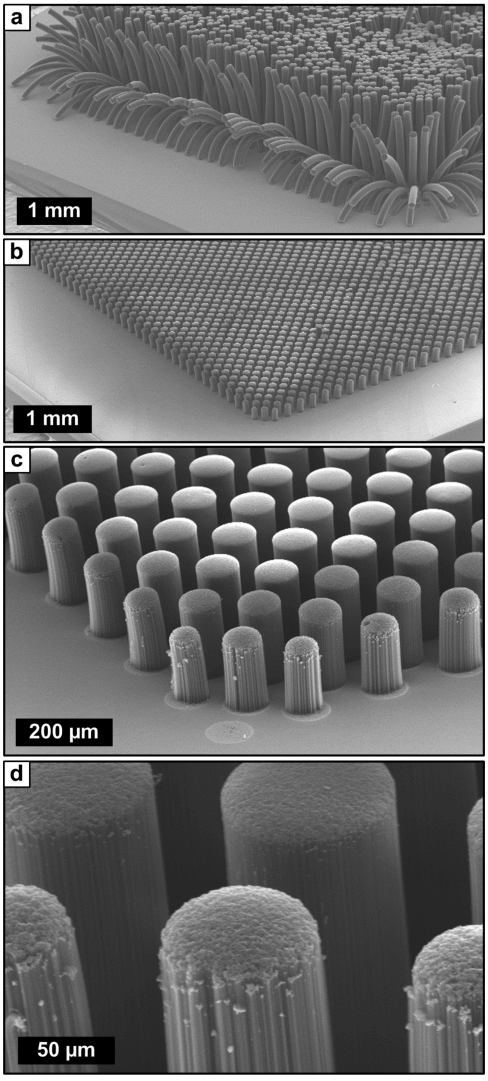

Figure 1. Nonuniformities in the geometry and dimensions of cylindrical CNT forest micropillars (100 μm diameter, 100 μm spacing in a square lattice). (a) Outward bending of peripheral micropillars in a large array, after growth time of 30 min. (b, c, d) Variations of height, diameter, and top surface geometry among CNT micropillars grown for only 3 min, under the same conditions as (a). Also note in (c) that the corner catalyst microfeature does not produce a CNT forest. This area has tangled CNTs, which fail to "lift off" into a forest. The same is observed around the perimeters of the micropillars along the edge of the array.

smaller diameter micropillars can be enhanced (*i.e.*, made taller and more uniform) by the presence of larger diameter micropillars or adjacent nonpatterned catalyst substrates placed in the CVD furnace to enhance growth.

These results imply that growth of CNTs is influenced by proximity effects of nearby CNTs and/or catalytically active surfaces that can influence the CVD environment. Recently, Parker *et al.* showed that placement of thin catalyst micropatterns adjacent to larger patterns influenced the smaller patterns and caused them to produce horizontally oriented CNT structures that bent away from the larger patterns.[13] Earlier, Borgstrom *et al.* demonstrated synergetic effects in gallium phosphide (GaP) nanowire growth, owing to both gas-phase and surface diffusion interactions influenced by the proximity and diameter of individual nanowires.[14]

For CNT growth by CVD, Bronikowski suggested that growth-promoting byproducts are generated during decomposition of the feedstock gas in areas of high catalyst concentration.[15] Jeong *et al.* proposed that the variation of local partial pressures of carbon-containing active gaseous precursors causes such catalyst proximity effects that lead to spatial variations in CNT forest height.[12] In addition, the curvature of the top surface of CNT micropillars has been attributed to the mechanical constraint of the tangled "crust" of the forest, coupled with spatial and temporal evolution of the CNT growth rate.[9] Nevertheless, there is no quantitative understanding of how and why catalyst proximity influences CNT growth. Reaching such an understanding is difficult due to the multicomponent nature of the CNT growth atmosphere and the existence of multiple chemical species having varying potency for promoting and/or deactivating the growth process.

During a typical CVD process for CNT growth, the hydrocarbon feedstock gas and byproducts of its gas-phase reactions[16−18] catalytically decompose at the surface of the catalyst nanoparticles, producing active species that promote the CNT growth process. Literature abounds with studies aiming at determining the activity of different carbon-containing species.[19] For instance, acetylene,[20] or alkynes in general,[18] and polycyclic aromatic hydrocarbons (PAHs)[21] have been identified as key active molecules in the CVD growth of CNTs. The efficiency of different hydrocarbon precursors is likely dependent on temperature, pressure, humidity, or the cooperative effects among multiple hydrocarbon precursors. It has also been proposed that polyaromatic intermediate fragments first form on the surface of the support layer in the vicinity of the catalyst before getting incorporated into the growing CNT.[22] These complex mechanisms are not fully understood, but they strongly suggest that chemical coupling is a fundamental aspect of CNT growth, and the cooperation of multiple chemical species with one another, the substrate, and the catalyst influences the growth rate and perfection of CNTs.

Therefore, to enable the manufacturing of uniform CNT forests and microstructures, we believe that a mathematical model is needed to describe the chemical process that involves local reactions at the nanoscale catalyst sites and their diffusion-induced coupling among the growing patterned structures at the microscale. Process uniformity is also a paramount issue in semiconductor manufacturing, and further analogies can be drawn for example to thickness variations in chemical−mechanical polishing[23] or the local variations of plasma etch rates.[24] In these cases,

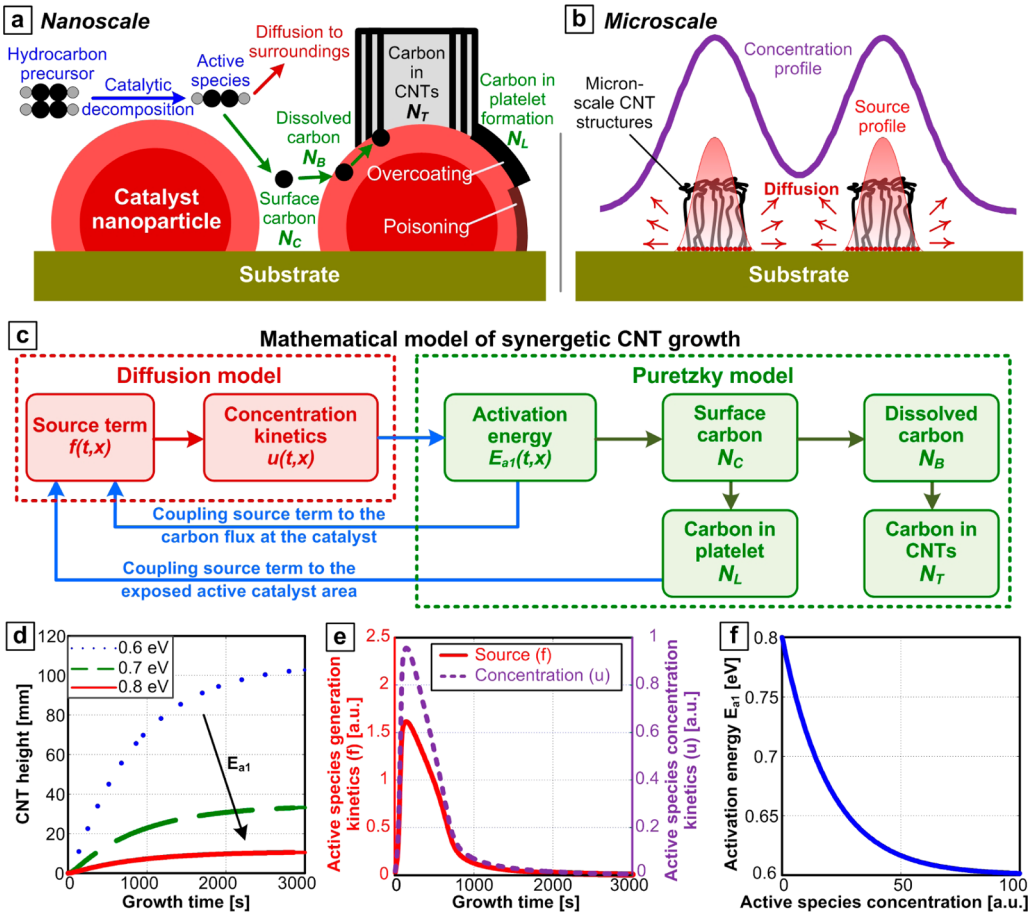

Figure 2. Model of synergetic CNT growth from the nanoscale to the microscale: (a) Schematic of the physical and chemical steps that lead to individual CNT growth from a catalyst nanoparticle on a substrate (adopted from Puretzky *et al.*[27]). (b) Schematic showing the diffusion-driven profile of active species, which is generated from the byproducts of the CNT growth reaction at the catalyst. (c) Block diagram of the chemically coupled synergetic CNT growth model, with feedback between the nominal CNT growth process and the diffusion of catalyst-generated active species. (d) Time-evolution of height for a 10 nm diameter CNT with different activation energies E_{a1}, without chemical coupling. (e) Kinetics of the source term and the ensuing concentration increase on the catalyst region, according to eqs 8, 9, and 10. The spatial step size is $\Delta x = 0.004$ mm, and the time step is $\Delta t = 7.5$ s. (f) Dependence of activation energy (E_{a1}) on the concentration of active species (u).

mathematical models of the coupling phenomenon have facilitated the design of patterns and process conditions to improve uniformity.

We present a hierarchical framework for modeling chemically coupled CNT growth, wherein a growth model for an individual CNT is modified to account for diffusion-induced spatial variations of growth behavior among arrays of CNT micropillars in proximity. We first model the spatial distribution of active species, which are generated at catalyst sites and diffuse to the surroundings. Owing to the autocatalytic nature of growth,[25,26] the activation energy of CNT growth is inversely related to the concentration of these active species, leading to a spatial correlation between concentration of active species and the modulation of CNT growth rates. Through simulations and experiments, we predict spatial variations according to pattern size and spacing, and we use these results to elucidate the successive stages of CNT micropillar lift-off in arrays. We demonstrate that this model can be used to design the CNT micropillar spacing and/or size in an array in order to enhance uniformity, in spite of collective chemical effects.

CHEMICALLY COUPLED CNT GROWTH MODEL

We developed a mathematical model of the synergetic growth of CNTs on a planar substrate. This model calculates the spatial distribution of active species that are locally produced at the catalyst surface and then diffuse to the surroundings (Figure 2a). Our approach is justified based on the knowledge that thermal and catalytic reactions involving the feedstock gas ethylene (C_2H_4) mixed with H_2 and He produce a variety of hydrocarbon species,[16] many of which contribute to the CNT growth process. It is most likely that a combination of gases, in addition to short-lived radicals, contribute to CNT growth. The reaction kinetics certainly depend on the temperature, pressure, and the catalyst nanoparticle composition, size, and shape.

To maintain generality, we collectively identify this combination of CNT growth precursors as "active species", without specifying a specific hydrocarbon

molecule/radical. The spatially varying concentration of these active species is utilized as a quantitative measure of chemical coupling, as it modulates the CNT growth rate by shifting the apparent activation energy of CNT growth. The diffusion of these active species over the CNT growth substrate results in a time-varying spatial distribution of concentration (Figure 2b), which supplements the nominal concentration of feedstock provided by the CVD system. The net concentration of active species, in combination with the other growth conditions, determines the CNT growth rate locally at each time step, enabling time-resolved simulations of the height evolution of the patterned CNT forest.

To model the chemical coupling between growing CNT micropillars, we combine a model of gas diffusion to a widely accepted model of CNT growth from a catalyst particle, which was developed by Puretzky *et al.*[27] Moreover, our synergetic growth framework (Figure 2c) is, in principle, compatible with any model of CNT growth that has a quantitative formulation of activation energy. Puretzky *et al*. model CNT growth as a sequence of physical and chemical steps: the chemisorption and catalytic decomposition of feedstock gas, the dissolution and diffusion of carbon on the nanoparticle surface, and, finally, the precipitation of carbon atoms into a growing CNT at the CNT−catalyst interface (Figure 2a). We model the spread of the chemical byproducts using a gas diffusion equation and, hence, calculate the time-evolving spatial distribution of their concentration. Each micrometer-scale catalyst area acts as a time-varying source of these active species, the kinetics of which is coupled to growth deactivation kinetics.

Recent research on CNT growth, especially for single-walled CNTs, has revealed more detailed mechanisms including the dynamic restructuring of nanoparticles during growth[28] and correlating the nucleation of CNT walls to both the phase[29] and lattice steps on the catalyst nanoparticle surface.[30] Moreover, the influence of chirality on both screw-dislocation-driven rotation of CNTs[31] and growth rate[32] was recently studied. Nevertheless, the Puretzky model is still generally applicable to growth of multiwalled CNTs by carbon diffusion and precipitation and reflects a general chemical process that is applicable to CNT growth without regard to diameter or chirality.

In our framework, the Puretzky model is first used to calculate the growth rate of an individual CNT. In this model, growth occurs from a metal catalyst nanoparticle (Figure 2a), which is surrounded by a carbon-containing gas feedstock as well as the products of thermal decomposition of the feedstock. These hydrocarbons catalytically decompose on the catalyst surface to atomic carbon and/or bonded carbon. The surface carbon then dissolves into a molten/disordered layer of the catalyst and precipitates, forming the growing CNT. In addition, some products of gas pyrolysis directly contribute to the formation of a carbonaceous platelet layer on the catalyst surface. Eventually, this platelet completely covers the catalyst nanoparticle, causing complete cessation of growth. The surface carbon can also incorporate into the carbonaceous layer, and the carbonaceous layer can dissolve into the molten layer.

The number of carbon atoms on the surface of the catalyst is denoted N_C, the number of carbon atoms in a poisoned layer (N_{L2}) or carbonaceous layer (N_{L1}) is collectively denoted as N_L, the number of atoms in a disordered layer of the catalyst is denoted as N_B, and the number of atoms in a growing nanotube is denoted as N_T. In the model used here, Puretzky *et al*. neglect the catalyst deactivation by poisoning, described as N_{L2},[27] and we also choose to consider that the only growth deactivation mechanism is catalyst overcoating with a carbonaceous layer N_{L1} (denoted here as N_L).

The carbon kinetics is given by a system of ordinary differential equations (ODEs):

$$\frac{dN_C}{dt} = \widetilde{F_{c1}}\, n\left(1-\frac{N_L}{\alpha S_0 n_m}\right) - (k_{sb}+k_{cl})N_C \quad (1)$$

$$\frac{dN_L}{dt} = \widetilde{F_{c2}}\, n_p\left(1-\frac{N_L}{\alpha S_0 n_m}\right) + k_{cl}N_C - k_{d1}N_L \quad (2)$$

$$\frac{dN_B}{dt} = k_{sb}N_C - k_t N_B + k_{d1}N_{L1} \quad (3)$$

$$\frac{dN_T}{dt} = k_t N_B \quad (4)$$

$$N_C(0) = N_L(0) = N_B(0) = N_T(0) = 0 \quad (5)$$

Here, n is the concentration of feedstock molecules, n_p is the concentration of gas-phase pyrolysis products, α is the number of monolayers coating the catalyst, n_m is the surface density of a monolayer of carbon atoms, S_0 is the surface area of the catalyst, k_{sb} is the rate constant of dissolution of carbon atoms, k_{cl} is the rate constant of formation of the carbonaceous layer, k_{d1} is the dissolution rate constant of the poisoning carbonaceous layer, and k_t is the rate constant of precipitation of carbon atoms into the nanotube.

The fluxes in eq 1 and eq 2 are given by

$$\widetilde{F_{c1}} = \frac{F_{c1}}{n},\ \widetilde{F_{c2}} = \frac{F_{c2}}{n_p} \quad (6)$$

$$F_{c1} = F_{b1}p_1 \exp\left(-\frac{E_{a1}}{k_B T}\right),$$
$$F_{c2} = F_{b2}p_2 \exp\left(-\frac{E_{a2}}{k_B T}\right) \quad (7)$$

$$F_{b1} = \frac{1}{4}S_0 n\left(\frac{k_B T}{2\pi m}\right)^{1/2},\ F_{b2} = \frac{1}{4}S_0 n\left(\frac{k_B T}{2\pi M}\right)^{1/2} \quad (8)$$

Here, p_1 and p_2 are pre-exponential factors. k_B is Boltzmann's constant, and T is the gas temperature. E_{a1} and E_{a2} are the activation barriers for catalytic decomposition and dissolution of the feedstock hydrocarbon, respectively. The masses of the feedstock molecule and the main pyrolysis product are denoted m and M, respectively. Values for n, n_p, S_0, T, m, and M were set to match the growth parameters of our experiments. The values selected for the other constants have been previously shown to agree with experimental results.[27,33] This system of ODEs is solved using Matlab's ode23s function.

As an example output of the uncoupled CNT growth model, the time evolution of CNT height and growth rate for a 10 nm diameter CNT grown at 1000 K from acetylene (C_2H_2) is shown in Figure 2d. The predicted growth rate (CNT height kinetics) reaches its maximum value very quickly, after a brief incubation period, and then gradually decays to zero. Lower activation energy leads to faster growth rate and greater terminal height (CNT length), as shown in Figure S1.

Now, to compute the rate of production of active species (source term kinetics shown in Figure 2b) on the catalyst surface, we couple it to the kinetics of surface carbon (N_C), which changes with time owing to the evolution of the overcoating layer (N_L). We model the source term in eq 9 as being proportional to $\widetilde{F_{c1}}\, n(1 - (N_L/\alpha S_0 n_m))$, *i.e.*, the positive term of the rate of change in surface carbon dN_C/dt eq 1. This source term (f) is now dependent on the available exposed catalytic surface area (*i.e.*, it represents the activity of the catalyst nanoparticle), which describes the kinetics of the generation of active species at the catalyst.

Therefore, the rate of active species generation is calculated for each CNT micropillar separately depending on position on the substrate (x,y) and time t by

$$f = \sum_i k_2 F_{c1,i}(t)\left(1 - \frac{N_{L,i}(t)}{\alpha S_0 n_m}\right)\chi_i(x,y) \qquad (9)$$

Here, χ_i represents the indicator function of the ith catalyst region, *i.e.*, a function with the value 1 for coordinates in this catalyst region and 0 elsewhere. The index i in $F_{c1,i}$ and $N_{L,i}$ specifies that these quantities are associated with the ith catalyst region. The constant k_2 is a scaling factor that is determined empirically by comparing simulations to experimental results. The time-dependent evolution of the source is shown in Figure 2e, where the source kinetics (f) at a single micropillar in a catalyst pattern decays to zero at growth termination. This source term is nonzero only at the catalyst regions and is zero elsewhere on the substrate.

Two more important assumptions are made. First, we assume that the distribution of the generated species over each microscale catalyst region is uniform, neglecting the synergetic growth effects among nanoscale catalyst particles within each region. Second, we assume that the concentration of the active species equals zero at the edge of the simulation space. In reality, the concentration on the boundary is nonzero due to the bulk concentration of precursor in the CVD system. In order to minimize the effect of this boundary condition on our simulation results, we use a domain size of 1 × 1 mm that is 10-fold larger than the maximum spacing between microscale catalyst features in our study (100 μm).

After the active species is produced at a catalyst region, it diffuses through the surrounding area. The concentration of the active species u is given by the diffusion equation, which is a partial differential equation that involves the source term f and the diffusion coefficient D,

$$\frac{\partial}{\partial t}u(x,t) = D\Delta u(x,t) + f(x,t) \qquad (10)$$

$$u(x,0) = 0 \qquad (11)$$

$$u(x,t) = 0 \text{ on the boundary} \qquad (12)$$

We solve the diffusion equation numerically by discretizing the spatial domain into a regular square lattice with step size Δx and discretizing time into equal time steps Δt. The Laplacian is discretized with a five-point stencil, and the equation is evolved using an implicit scheme with a conjugate gradient solver. At each time step, the source term f is calculated from the concentration N_L, which is found by solving eqs 1−5 on the time interval $[t,t+\Delta t]$ with Matlab's ode23s solver. The step size Δx is chosen small enough that each catalyst region is several grid points wide. We select a time step that balances accuracy and computation time. Moreover, there are no hard constraints on the time step Δt, because the implicit time-stepping scheme is unconditionally stable and the concentration u does not involve any fast dynamics.

The kinetics of the active species concentration is shown to closely follow the source kinetics for the same CNT micropillar (Figure 2e). This occurs because the diffusion of the gas is relatively fast in comparison to the time scale of CNT micropillar growth.

A final important detail of our model is the coupling of active species concentration to the activation energy, which modulates the CNT growth kinetics according to the local concentration of active species. As the concentration of the active species increases, the growth rate of the CNTs also increases; that is, the activation energy E_{a1} in the Puretzky model decreases. Hence, our model is based on modulating this activation energy E_{a1} by mathematically coupling it to the average concentration $\bar{u}$ of active gaseous species on each catalyst region, as shown in eq 14,

$$\bar{u}_i(t) = \frac{\int u(x,t)\,\chi_i(x)\,dx}{\int \chi_i(x)\,dx} \qquad (13)$$

$$E_{a1,i}(t) = E_{min} - (E_{max} - E_{min}) \exp(k_1 \bar{u}_i(t)) \quad (14)$$

Here, χ_i represents the indicator function of the ith catalyst region. When the active species concentration is zero, $E_{a1} = E_{max}$; when the concentration is large, E_{a1} approaches the asymptote E_{min}. The constants E_{min} and E_{max} are chosen based on values from the work by Puretzky *et al.*,[27,33] while the constant k_1 is chosen as the value for which the relative heights of CNTs in the simulations are consistent with those obtained in our experiments. Figure 2f shows a plot of the dependence of E_{a1} on u when $E_{max} = 0.8$, $E_{min} = 0.6$, and $k = 0.05$. eq 14 captures the three main features of such dependence. The first feature is the inverse relation between concentration and activation energy. The second feature is having a maximum for activation energy at zero concentration, *i.e.*, in the absence of catalytically produced active species diffusing from the surroundings. In this case, this value of maximum activation energy results from only the active species produced by thermal decomposition of the hydrocarbon feedstock and those that are locally generated at the catalyst location (with no contribution from the surroundings). These are dependent on CVD conditions including the precursor chemistry, temperature, and residence time and are independent of the catalyst microscale pattern. The third feature is the presence of a minimum bound for the activation energy that cannot be surpassed no matter how high the concentration of the active species gets. This is mathematically described as an asymptote of the exponential function. This phenomenological relationship is also consistent with the experimental observations obtained for the dependence of growth rate of nanowires on the spacing, in which experimental results of growth rates exhibited a maximum at small spacing and decayed to an asymptotic minimum.[14]

Last, note that the height of the CNT forest is adopted as a quantitative measure of the efficiency of the CVD process. We assume that all CNTs within a forest (micropillar) are identical and are mechanically coupled, and therefore collectively grow at the same rate.[34] As a result, the model predicts only the straight vertical growth of each micropillar. The spatial variations of CNT growth rate within each micropillar and the resulting deformation during growth (*e.g.*, Figure 1a) are topics of ongoing research in our group, and modeling-coupled mechanochemical effects are beyond the scope of the present work.

RESULTS

The comprehensive growth model described above provides a framework to simulate the influence of chemical coupling on CNT growth and can be correlated with experimental results, which in turn inform the model and enable validation of improved growth conditions. In the subsections that follow, we show that the chemically coupled model predicts spatial nonuniformities in CNT growth rate among micropillar arrays (Figure 4 and Figure 5). We also show that the "digital" change in CNT growth from tangled horizontal mat to vertically aligned forest can be explained based on a threshold concentration of active species (Figure 5 and Figure 6). Moreover, we exploit the insights gained by our simulation and experimental results to design more uniform individual CNT micropillars (Figure 7), as well as more uniform micropillar arrays (Figure 8).

Diffusion-Driven Concentration Profiles. First, we use the model to visualize and understand how the diffusion of the active species (gas) depends on the CVD conditions and the pattern design. The diffusion coefficient (D) in eq 10 depends on temperature, pressure, and the gases. For example, the diffusion coefficient of C_2H_4 in He at 1 atm was calculated to be 1 cm^2/s at 600 K and 2 cm^2/s at 1000 K, according to an empirical relation (Figure S2).[35] We first show the effect of process temperature on gas diffusion and the resulting spatial distribution of active species concentration. Concentration profiles are plotted in Figure 3 after 750 s of growth at two different temperatures of 600 and 1000 K, which correspond to the values of diffusion coefficient of 1 and 2 cm^2/s, respectively. As shown in this figure, the maximum concentration occurs at the center micropillar in a hexagonal array, because at this location the maximum number of micropillars contributes to the overall concentration of active species. Higher pressures and lower temperatures significantly reduce gas diffusion to the surroundings, resulting in a much higher local concentration of active species. Also, for patterns with larger spacing (δ), the local maxima in the concentration profile are sharper, in contrast to the smooth concentration profiles observed for closely packed catalyst microfeatures.

Predicting Spatially Varying CNT Growth Kinetics. Now, we show that the spatial distribution of active species governs the growth kinetics of CNT micropillars in arrays, predicting the observed dependence of CNT growth rate and terminal height. A 3D plot of the normalized terminal height of an exemplary CNT micropillar array (Figure 4a) shows that the array has a domed shape with taller micropillars toward the center and shorter micropillars at the edges. As a control case, an array simulation without chemical coupling, resulting in perfect uniformity, is shown in Figure S3. In Figure 4b the height kinetics of the central micropillar and the corner micropillar are shown, revealing that the final height of the corner micropillar is about 60% of the final height of the central micropillar. This height difference is present because the spatial variation of active species modulates the activation energy (Figure 4c) for the CNT growth process, by the formulation discussed previously.

The kinetics of the active species generation at the central micropillar are shown in Figure 4d, and the kinetics of active species concentration are shown

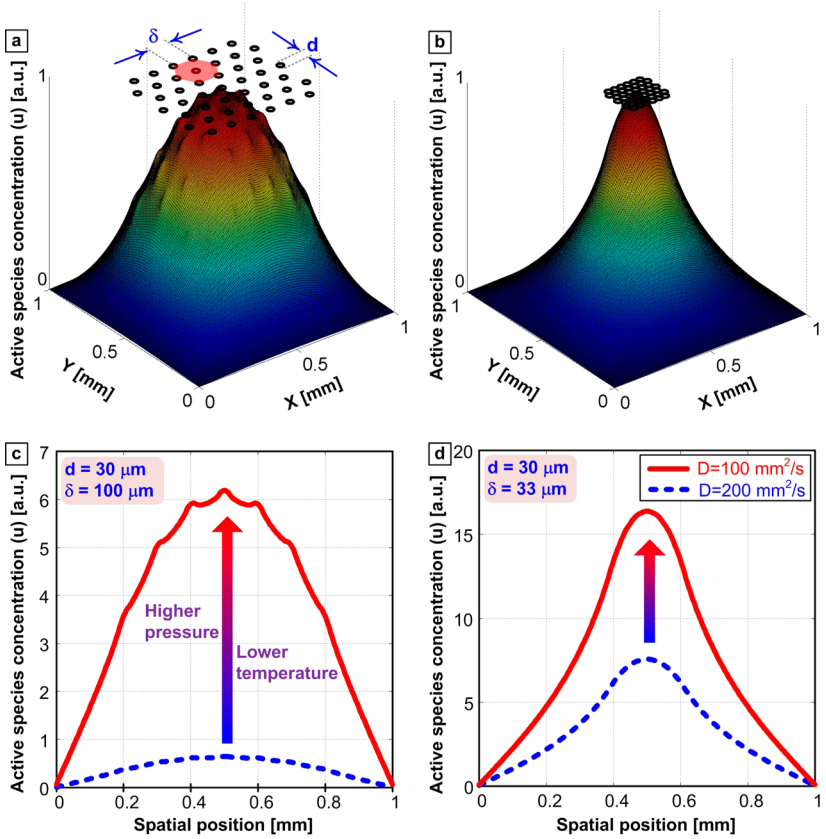

Figure 3. Influence of model parameters on the spatial distribution of active species generated within and around a CNT growth pattern. (a, b) 3D surface plot of concentration profile of active species generated at micrometer-scale catalyst patches (d = 30 μm) that are arranged in a hexagonal array with different spacing (δ) of 100 and 33 μm, respectively (diffusion coefficient D = 100 mm^2/s). (c, d) 2D spatial distribution of active species concentration (u) for the same two catalyst arrays, plotted after 750 s of growth for two different temperatures of 600 and 1000 K, which correspond to diffusion coefficients of 100 mm^2/s and 200 cm^2/s, respectively. The spatial step size is Δx = 0.004 mm, and the time step is Δt = 7.5 s.

in Figure 4e. After a rapid increase, the production rate decreases almost linearly and then decays exponentially to zero. The spatial profiles of the active species generation and the ensuing concentration at t = 750 s are shown in Figure 4f,g. The growth rate is typically lower at the edge of the pattern because the higher activation energy there causes carbon to decompose at a lower rate, and therefore the active species are produced at a lower rate (Figure 4g). Shallow peaks in active species concentration are observed at the catalyst site locations, where the gas is consumed by CNT growth. The maximum concentration occurs at the center of the array, and the concentration decays to zero at the end points, representing the boundary of the simulation space.

We now compare simulations to experiments to understand the synergetic growth effects within an array of CNT micropillars. SEM images (Figure 5a–c) show that the height and uniformity of 30 μm diameter CNT micropillars decrease as the spacing between the catalyst microfeatures increases. Specifically, for small spacing (center-to-center distance of 33 μm), all CNT micropillars in the array grow vertically upward. In the case of large spacing (100 μm), none of the catalyst features produce a sufficient density of CNTs to lift off and grow vertically. For the array with medium spacing (60 μm), only the CNT micropillars toward the center of the array grow vertically, while features toward the edges/corners of the array do not grow vertically. This consistent observation can be explained by the spatial variation of concentration-modulated growth that gives rise to the height variation shown in Figure 4. However, to this point, the model does not explain the abrupt transition between features that do not grow vertically and those that produce vertical CNT forests.

Predicting a Chemical Threshold for CNT Forest Growth. The catalyst microfeatures that do not grow vertically aligned CNTs exhibit a lower density of tangled CNTs (inset in Figure 5c). Previous work, using X-ray scattering to profile the density of CNTs within a forest grown to termination, showed that a threshold CNT density is needed to create and maintain the vertically aligned forest structure.[26,36] This threshold density was also predicted by finite element modeling of the CNT crowding mechanics.[37] Therefore, we hypothesize that the time-varying (increasing) concentration of active species that results from diffusion across the substrate drives the kinetics of CNT density increase and

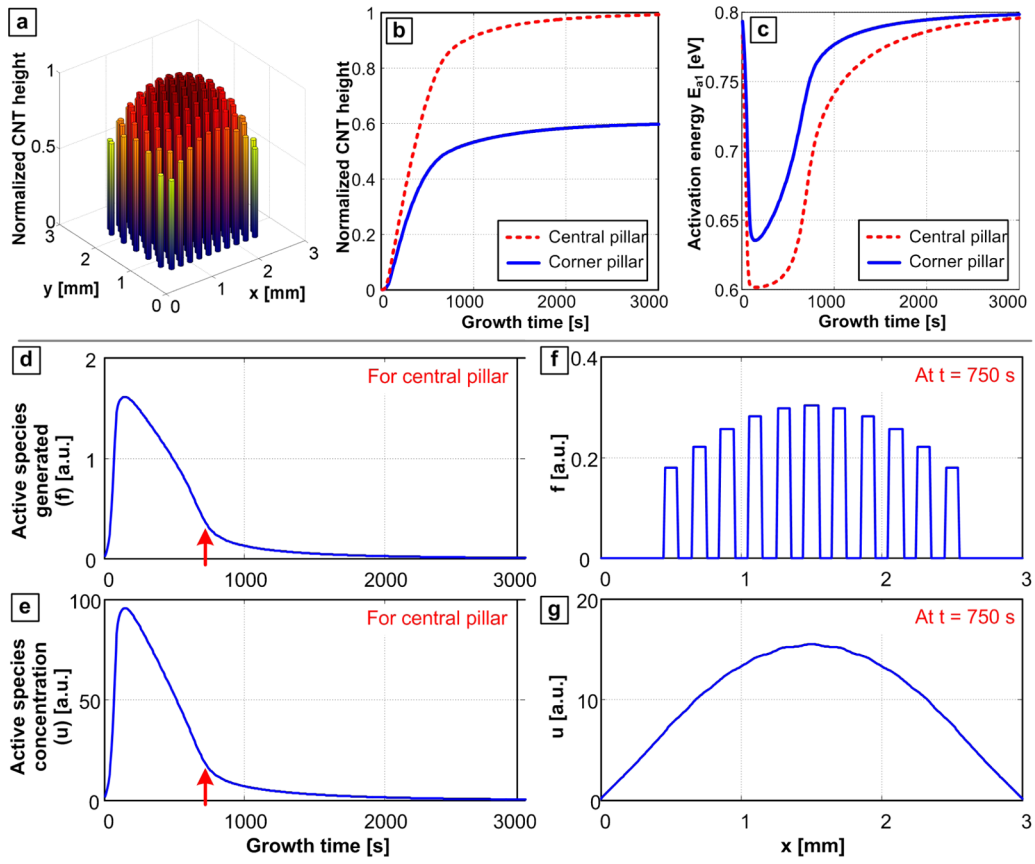

Figure 4. Simulation results for a hexagonal array of CNT micropillars d = 100 μm and δ = 200 μm center-to-center spacing. The spatial step size is Δx = 0.012 mm, and the time step is Δt = 7.5 s. (a) 3D plot of the spatial distribution of normalized micropillar heights. (b) Height kinetics for the central micropillar and a corner micropillar. (c) Time evolution of activation energy (E_{a1}). (d, e) Time evolution of the active species generation term (source term) and the ensuing concentration for the same central micropillar. (f, g) Spatial distribution of the active species generation term (source term) and the concentration distribution after 750 s of growth (at y = 1.5 mm).

eventual forest lift-off. We explain the transition between tangled and vertical CNTs (Figure 5d−f) by a threshold concentration of active species (Figure 5g−i) that is necessary to cause the CNT density to surpass the threshold for self-organization into the vertically aligned forest morphology. Although some CNTs can start growing into a randomly oriented mat as soon as the hydrocarbon feedstock is introduced into the reactor (see inset in Figure 5i), vertical growth of the forest is delayed until the threshold concentration is reached, as shown in Figure 5j−l. The value of this threshold was chosen to match the experimentally obtained micropillar height distribution, and it would in principle depend on the overall area of the catalyst microfeatures and CVD conditions. Video animations showing the time evolution of concentration, along with the effect of thresholding, are available online as Supporting Information (videos S1−3).

Close-up electron micrographs of the CNT micropillar array with medium spacing (Figure 6a) show that the geometry of each micropillar is nonuniform as well; that is, the top surface of the micropillar can be curved and the pillar has a varying cross-sectional area from top to bottom. This nonuniformity, which is a typical indication of low-density CNT micropillars, can be attributed to density profiles across the height of each micropillar.[26,37,38] Although these density variations are not captured by our mathematical model, the introduction of the chemical threshold, shown in Figure 5g, h, i, adequately predicts the transition from horizontal randomly oriented growth of CNT mats to the vertical self-supported aligned growth of CNT forest morphology.

We can also infer the successive stages of vertical micropillar growth by examining micropillars at varying stages of growth based on their spatial position in the array. Figure 6b shows a schematic of the successive stages that are needed for CNT micropillar lift-off. First, CNT nucleation starts as soon as the hydrocarbon gas feedstock is introduced to the reactor; yet at this stage CNTs grow in random orientations, forming a tangled 2D mat. This crowding stage proceeds until the density of growing CNTs reaches a threshold value, which has been previously identified to be about 10^9 CNTs/cm^2 for CNTs grown by the same CVD recipe.[26,37] This threshold density represents the density at which the total upward force overcomes the van der Waal's attraction forces pulling the CNTs to the substrate.

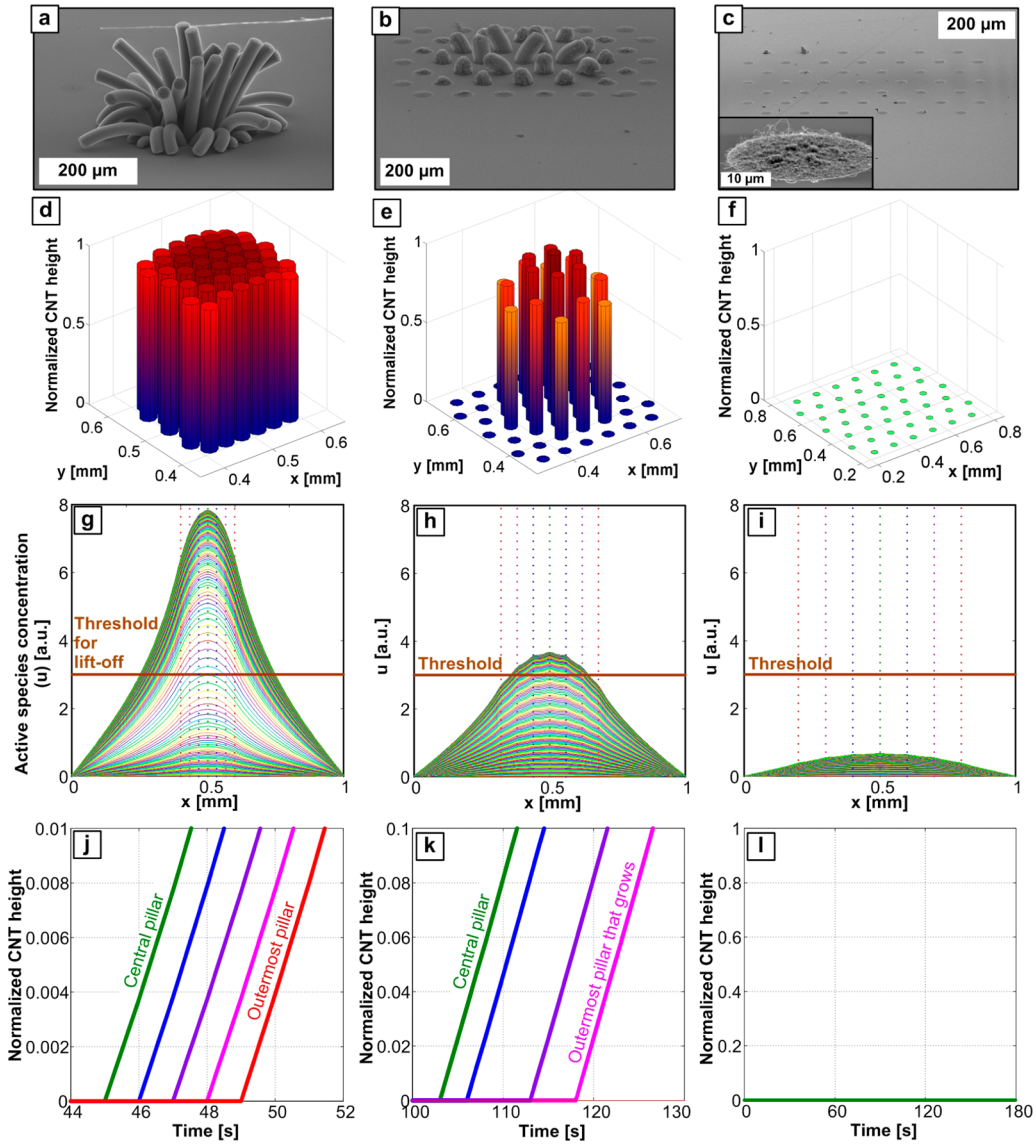

Figure 5. Effect of micropillar spacing in arrays on lift-off and growth. SEM images of CNT micropillar arrays having center-to-center pillar spacing of 33, 60, and 100 μm are shown in (a, b, c), respectively. The inset to (c) shows a tangled mat of CNTs in cases when the micropillars do not lift off into a forest. Simulation results showing relative heights for these different CNT spacings are plotted in (d, e, f). The spatial step size is Δx = 0.004 mm and the time step is Δt = 1.0 s. Time evolution of the spatial distribution of active species concentration for different spacings is plotted in (g), (h), and (i), identifying the threshold for lift-off. A plot of the initial CNT forest height kinetics for each spacing is plotted in (j), (k), and (l), showing the delayed onset of lift-off for outer micropillars compared to the central micropillar. The position of the threshold relative to the active species concentration indicates whether or not the CNT micropillar has lifted off into a forest; specifically, the model of the array in (a) predicts accurately that all the CNT pillars lift off, and the model of (c) predicts that the active species never crosses the threshold due to the larger spacing and reduced chemical coupling.

Although our mathematical model considers that the rate of active species generation is constant across each micrometer-sized catalyst area (Figure 2b), there are likely local rate variations due to the chemical coupling between individual catalyst nanoparticles within the catalyst area. Hence, we expect that the CNT activation kinetics is fastest toward the middle of the catalyst area for each micropillar. As a result, the threshold density is reached in the middle of the micropillar area first, and lift-off starts to develop from the center of the micropillar, until, eventually, the whole micropillar lifts off. This delay between the lift-off of the middle portion of the micropillar and the lift-off of the whole micropillar results in a dome-shaped top surface. For instance, a more curved top is an indication of slow kinetics of CNT activation as the active species propagates through the micropillar. Our model does not describe the curvature of the top surface of the pillar, because the height kinetics is assumed to be similar for all CNTs within each micropillar. Nevertheless, the explanation above, which can be mathematically modeled in the future, provides insights into the kinetics of CNT self-organization that are necessary to establish vertical growth.

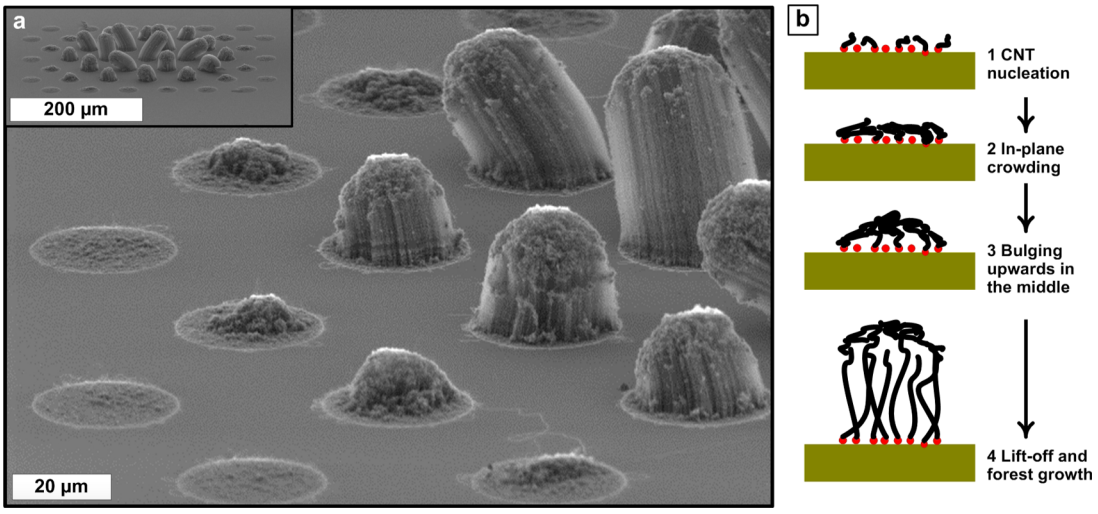

Figure 6. Analysis of the CNT growth gradient at the edge of a micropillar array and identification of successive stages of micropillar lift-off due to collective chemical and mechanical effects. (a) SEM of the medium spacing array (with 60 μm spacing), showing that micropillars are at different stages of lift-off depending on their position in the array. (b) Schematic showing the progression of stages leading to CNT micropillar lift-off.

Design of Uniform CNT Micropillars. The capability to predict CNT growth patterns can also enable engineering of process conditions and pattern geometries to achieve improved uniformity. One way to achieve geometric uniformity for individual catalyst microfeatures that typically do not grow into tall, straight micropillars is to add a border of CNTs around the feature. Figure 7 shows the effect of having a surrounding border of CNTs around a 30 $\times$ 30 μm square micropillar. For a small spacing of 100 μm between the central micropillar and the border, the resulting central micropillar is straighter than in the case of the larger spacing (300 μm). Also, the geometry of the top surface of the micropillar is more uniform and square in the case of the smaller spacing, compared to a more curved top in the case of the larger spacing. This is attributed to the faster kinetics of CNT activation that result from the higher concentration of active species in the case of smaller spacing (Figure 7b), owing to the external supply (from the border) of active species to the otherwise isolated micropillar. This finding is consistent with a recent study, in which an outer surrounding border was shown to improve the straightness and alignment of CNT microstructures grown for microelectromechanical systems (MEMS) applications.[39]

Additionally, applying the insights from our simulations and experiments, CNT micropillar uniformity can be engineered by designing the array patterns. Tailoring the spacing between micropillars and/or the size of individual micropillars results in a more uniform distribution of active species concentration, which in turn improves the uniformity of CNT micropillar height. Figure 8 shows strategies that can greatly enhance the height uniformity. The first strategy (Figure 8b, e) features a spatially varying spacing, where the distance between micropillars is largest in the middle of the array and smallest at the periphery of the array. This strategy is helpful for those applications that require similar diameter micropillars without requiring that the positions of micropillars are equally spaced. The second strategy (Figure 8c, f) relies on changing the cross-sectional dimensions (area) of the micropillars across the array, wherein pillars toward the center of the pattern are smallest and micropillars toward the periphery of the pattern are largest. This strategy is suitable for applications in which the position, or the center-line, of each micropillar is prespecified by the device design, such as in the case of growing CNT micropillars to connect circuits having multiple layers. In both strategies, the concentration profile becomes more uniform, as compared to the case of a uniformly spaced same-sized micropillar array.

For the second strategy the total catalyst area is increased, which results in an increase in the magnitude of the produced active species and is, therefore, likely to be accompanied by an increase in CNT activation rate and density. Simulation results show that the ratio between the shortest (outermost) micropillar and the tallest (central) micropillar has increased from 86% in the case of uniformly spaced same-sized micropillars to 92% by applying the first strategy (varying the spacing only) and to 93% by applying the second strategy (varying the micropillar size only). Hence, employing a combination of similar strategies in pattern design will both homogenize the typically nonuniform concentration profile of active species and boost the density activation kinetics of CNT micropillars.

DISCUSSION

Prior work in the literature has shown that CNT growth can be limited by gas diffusion of the precursor.[40,41] Our framework considers the dynamics of

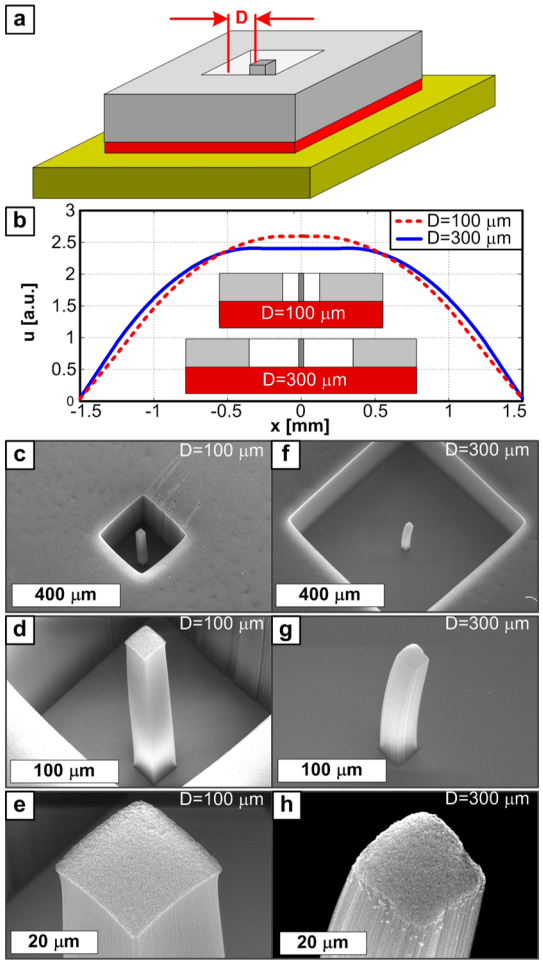

Figure 7. Realization of isolated straight CNT micropillars (30 × 30 μm) using a border feature to augment the active species concentration. (a) Schematic of design. (b) Concentration profile of active species showing two cases with different spacing D (100 and 300 μm). The spatial step size is Δx = 0.012 mm, and the time step is Δt = 7.5 s. SEM images at different magnifications for the 100 μm spacing (c–e) and the 300 μm spacing (f–h).

gas diffusion of hydrocarbon species generated at the catalyst sites, which results in a time-evolving concentration profile. Although we consider that the rate-limiting process in CNT growth is gas diffusion, we formulate the effect of the ensuing concentration profile on the catalytic decomposition of hydrocarbons at the catalyst. Our modeling framework consolidates into a single metric the various gaseous species that modulate the reaction activation energy of hydrocarbon dissociation on the surface of catalyst nanoparticles (E_{a1}). Previous work has shown that CNT growth could be limited by the diffusion of carbon atoms into/on the catalyst nanoparticle,[42] which would require coupling the energetics/kinetics of carbon dissolution to concentration u, but this effect is ignored in the present work.

The concentration of an individual hydrocarbon precursor should not change the activation energy for chemical decomposition on the catalyst surface (E_{a1}). However, there is a preponderance of evidence that a family of hydrocarbon gases and radicals contribute to CNT growth by thermal CVD, and these have varying potency in promoting CNT growth. As the concentration and distribution of these precursors change due to thermal and catalytic decomposition of the input feedstock, the collective activation barrier for chemical decomposition is shifted in the vicinity of the catalyst surface. Our model collectively approximates this effect by modulating the value of E_{a1} based on the concentration of generated active species (u).

Further research is required to enable a mathematical description of the relative proportions of each of these species, and designed experiments are needed to investigate their isolated, as well as cooperative, effects on modulating growth, as well as on activating CNT growth during the nucleation stage. In addition, the effects of other additives such as oxygen,[43] hydrogen,[43] water vapor,[8] and carbon dioxide[44,45] on mediating CVD growth of CNTs should be taken into consideration. Other gaseous species have an opposite effect on growth, and some species might play either an activating or deactivating role depending on their partial pressure, total pressure, temperature, and/or gas composition in the reactor. These "harmful" effects on growth should also be modeled, in order to describe the growth process more accurately. This activation/deactivation competition is not solely controlled by the byproducts of local catalytic reaction or even gas-phase reaction in the vicinity of the catalyst particle, but are also affected by the desorption of various species from the reactor wall.[46]

Despite such complexities and the assumptions of this study, we can make important quantitative insights regarding the influence of process parameters, such as temperature and pressure, on synergetic CNT growth. For instance, CNT growth at lower temperature and higher pressure increases the influence of chemical coupling, because sharper chemical gradients result from lower diffusion coefficients (Figure 3). On the other hand, high-temperature growth in low-pressure conditions should reduce synergetic growth effects due to the high diffusion coefficient and mean free path. Temperature variation would also affect the reaction kinetics, and that pressure variation would also influence the gas residence time, which is known to influence CNT growth independently of synergetic effects. Therefore, the mathematical framework for modeling chemical feedback on CNT growth will enable exploration of improved uniformity in future work.

CONCLUSIONS

We enable prediction and control of nonuniformities in as-grown CNT micropillars by developing a holistic mathematical model that couples isolated CNT growth with diffusion of reactive species across the substrate. This model replicates experimental findings where the

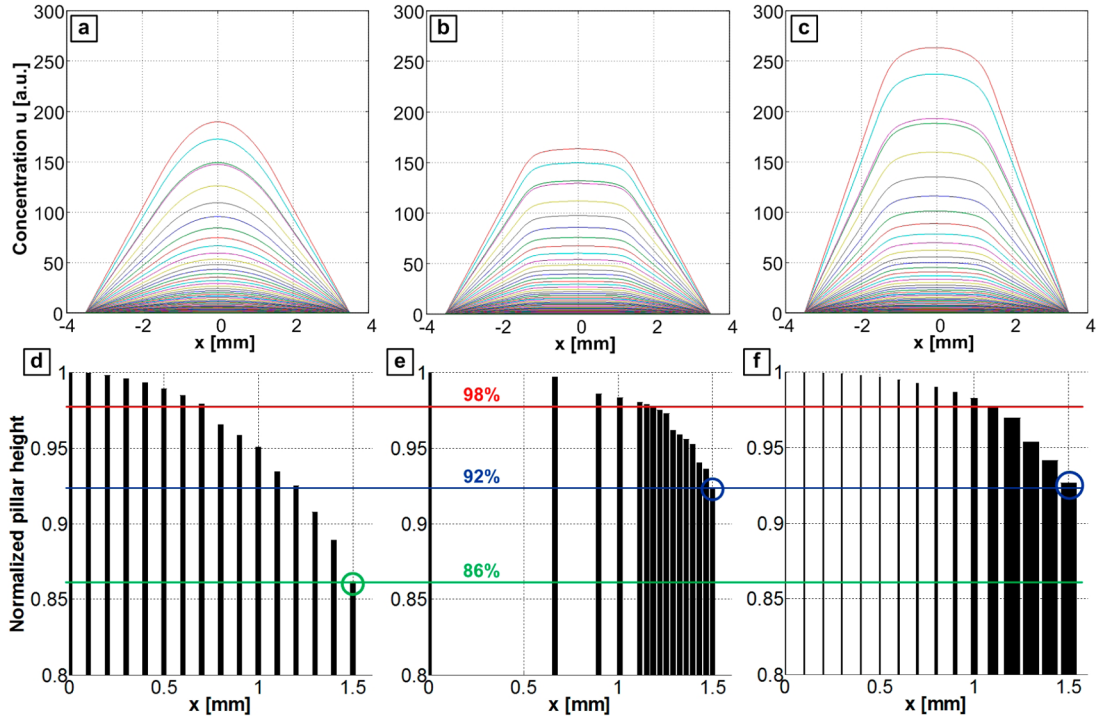

Figure 8. Predicted design of CNT micropillar arrays to achieve increased height uniformity in the presence of chemical coupling. Evolution of the spatial distribution of active species concentration is shown for (a) uniformly spaced (60 μm spacing) micropillars having the same width (30 μm), (b) nonuniformly spaced micropillars having the same width (30 μm), and (c) uniformly spaced micropillars having varying widths. Relative height distributions for only right-side half of the micropillar array for (a), (b), and (c) are shown in (d), (e), and (f), respectively. The spatial step size is Δx = 0.004 mm, and the time step is Δt = 7.5 s.

overall height and uniformity of CNT micropillars are influenced only by the spacing between catalyst microfeatures on the substrate. Combining experiments and simulations reveals that a threshold concentration of active species is needed for lift-off of CNT micropillars and corroborates analysis of the successive stages of CNT micropillar growth. Our findings also enable the design and fabrication of uniform micropillar arrays, which are essential for the scaled manufacturing of commercial CNT-based devices with enhanced electrical, thermal, and mass transport properties. An example of utility is presented *via* designs predicting a more uniform distribution of micropillar heights or designed height gradients. In the future, this approach could also serve as a basis for optimization algorithms for pattern design considering both chemical reaction models and synergetic coupling effects, with relevance to CNTs as well as other nanostructures by CVD reactions.

EXPERIMENTAL SECTION

Catalyst Patterning. Micron-scale patterning of the catalyst film was achieved by photolithography on a (100) silicon wafer with a 300 nm thermally grown SiO_2 layer. After spin-coating the photoresist (SPR220), a patterned mask was used during contact exposure of UV light (Karl Suss MA/BA-6) at 30 mJ/s for 6 s. After development of the patterned photoresist, the supported catalyst (1 nm Fe on 10 nm Al_2O_3) was deposited by sputtering (Lab 18 by Kurt J. Lesker). The wafer was diced manually by a diamond-tip scribe. The remaining photoresist was then lifted off the wafer by placing samples in an ultrasonic bath of acetone, before loading the catalyst-coated Si chips into the tube furnace.

CNT Growth and Characterization. CNTs were grown in a custom-built hot-wall tube furnace, with a rapid sample insertion mechanism. First, the substrate was annealed to induce catalyst film dewetting and nanoparticle formation in a reducing atmosphere of hydrogen and helium (400 sccm H_2/100 sccm He) at 775 °C (10 min ramp time and 10 min temperature hold). After the annealing step, the substrate was retracted from the reactor and held in an adjacent cold chamber, while introducing the feedstock gas, ethylene (C_2H_4), changing the gas mixture to the growth atmosphere (100 sccm C_2H_4/400 sccm He/100 sccm H_2) at the same temperature. After 7 min, during which the gases and the humidity inside the tube furnace stabilize, the substrate was returned to inside the reactor. CNTs were characterized by scanning electron microscopy (SEM), using a Philips XL30FEG.

Conflict of Interest: The authors declare no competing financial interest.

Acknowledgment. We thank Prof. Selim Esedoglu and Prof. Hayden Taylor for valuable discussions and Sei Jin Park for his comments on the manuscript. We also thank Dr. Alex Puretzky (ORNL) for providing the computer code for the mathematical model of CNT growth. Financial support to M.B. and A.J.H. was provided by the Department of Energy Office of Basic Sciences (DE-SC0004927), and to B.F. by the National Science Foundation (DMS-0748333). Experiments and characterization work was supported by the Department of Energy Office of Basic Sciences (DE-SC0004927). Catalyst deposition and lithography were carried out in the Lurie Nanofabrication Facility (LNF), and electron

microscopy was carried out in the Electron Microbeam Analysis Library (EMAL), both at the University of Michigan.

Supporting Information Available: Supporting Information includes plots showing the effect of changing both CNT diameter and activation energy on growth kinetics of CNTs according to the Puretzky model. Details of the calculation of the diffusion coefficient used in the mathematical model are included, showing the dependence of the diffusion coefficient on both the reactor temperature and pressure. A juxtaposition of simulation results of CNT micropillar array growth with and without taking into consideration synergetic coupling effects according to the proposed mathematical model. Videos showing the time evolution of active species concentration profiles and growth kinetics for CNT micropillar arrays having 33, 60 and 100 μm. This material is available free of charge *via* the Internet at http://pubs.acs.org.

REFERENCES AND NOTES

1. De Volder, M. F. L.; Tawfick, S. H.; Baughman, R. H.; Hart, A. J. Carbon Nanotubes: Present and Future Commercial Applications. *Science* **2013**, *339*, 535–539.
2. Hutchens, S. B.; Hall, L. J.; Greer, J. R. *In Situ* Mechanical Testing Reveals Periodic Buckle Nucleation and Propagation in Carbon Nanotube Bundles. *Adv. Funct. Mater.* **2010**, *20*, 2338–2346.
3. Maschmann, M. R.; Ehlert, G. J.; Park, S. J.; Mollenhauer, D.; Maruyama, B.; Hart, A. J.; Baur, J. W. Visualizing Strain Evolution and Coordinated Buckling within CNT Arrays by *in Situ* Digital Image Correlation. *Adv. Funct. Mater.* **2012**, *22*, 4686–4695.
4. Wei, B. Q.; Vajtai, R.; Ajayan, P. M. Reliability and Current Carrying Capacity of Carbon Nanotubes. *Appl. Phys. Lett.* **2001**, *79*, 1172–1174.
5. Tawfick, S.; O'Brien, K.; Hart, A. J. Flexible High-Conductivity Carbon-Nanotube Interconnects Made by Rolling and Printing. *Small* **2009**, *5*, 2467–2473.
6. Berber, S.; Kwon, Y. K.; Tomanek, D. Unusually High Thermal Conductivity of Carbon Nanotubes. *Phys. Rev. Lett.* **2000**, *84*, 4613–4616.
7. Yuan, G.; Marconnet, A. M.; Rong, X.; Maruyama, S.; Goodson, K. E. Heat Capacity, Thermal Conductivity, and Interface Resistance Extraction for Single-Walled Carbon Nanotube Films Using Frequency-Domain Thermoreflectance. *IEEE Trans. Comp. Packag. Technol.* **2013**, *3*, 1524–1532.
8. Hata, K.; Futaba, D. N.; Mizuno, K.; Namai, T.; Yumura, M.; Iijima, S. Water-Assisted Highly Efficient Synthesis of Impurity-Free Single-Walled Carbon Nanotubes. *Science* **2004**, *306*, 1362–1364.
9. Han, J. H.; Graff, R. A.; Welch, B.; Marsh, C. P.; Franks, R.; Strano, M. S. A Mechanochemical Model of Growth Termination in Vertical Carbon Nanotube Forests. *ACS Nano* **2008**, *2*, 53–60.
10. Vinten, P.; Bond, J.; Marshall, P.; Lefebvre, J.; Finnie, P. Origin of Periodic Rippling during Chemical Vapor Deposition Growth of Carbon Nanotube Forests. *Carbon* **2011**, *49*, 4972–4981.
11. De Volder, M. F. L.; Vidaud, D. O.; Meshot, E. R.; Tawfick, S.; Hart, A. J. Self-Similar Organization of Arrays of Individual Carbon Nanotubes and Carbon Nanotube Micropillars. *Microelectron. Eng.* **2010**, *87*, 1233–1238.
12. Jeong, G. H.; Olofsson, N.; Falk, L. K. L.; Campbell, E. E. B. Effect of Catalyst Pattern Geometry on the Growth of Vertically Aligned Carbon Nanotube Arrays. *Carbon* **2009**, *47*, 696–704.
13. Parker, J. M.; Wong, H. S. P. Synergetic Carbon Nanotube Growth. *Carbon* **2013**, *62*, 61–68.
14. Borgstrom, M. T.; Immink, G.; Ketelaars, B.; Algra, R.; Bakkers, E. P. A. M. Synergetic Nanowire Growth. *Nat. Nanotechnol.* **2007**, *2*, 541–544.
15. Bronikowski, M. J. CVD Growth of Carbon Nanotube Bundle Arrays. *Carbon* **2006**, *44*, 2822–2832.
16. Meshot, E. R.; Plata, D. L.; Tawfick, S.; Zhang, Y. Y.; Verploegen, E. A.; Hart, A. J. Engineering Vertically Aligned Carbon Nanotube Growth by Decoupled Thermal Treatment of Precursor and Catalyst. *ACS Nano* **2009**, *3*, 2477–2486.
17. Plata, D. L.; Hart, A. J.; Reddy, C. M.; Gscwend, P. M. Early Evaluation of Potential Environmental Impacts of Carbon Nanotube Synthesis by Chemical Vapor Deposition. *ACS Nano* **2009**, *43*, 8367–8373.
18. Plata, D. L.; Meshot, E. R.; Reddy, C. M.; Hart, A. J.; Gschwend, P. M. Multiple Alkynes React with Ethylene To Enhance Carbon Nanotube Synthesis, Suggesting a Polymerization-Like Formation Mechanism. *ACS Nano* **2010**, *4*, 7185–7192.
19. Kimura, H.; Goto, J.; Yasuda, S.; Sakurai, S.; Yumura, M.; Futaba, D. N.; Hata, K. Unexpectedly High Yield Carbon Nanotube Synthesis from Low-Activity Carbon Feedstocks at High Concentrations. *ACS Nano* **2013**, *7*, 3150–3157.
20. Eres, G.; Kinkhabwala, A. A.; Cui, H. T.; Geohegan, D. B.; Puretzky, A. A.; Lowndes, D. H. Molecular Beam-Controlled Nucleation and Growth of Vertically Aligned Single-Wall Carbon Nanotube Arrays. *J. Phys. Chem. B* **2005**, *109*, 16684–16694.
21. Nessim, G. D.; Seita, M.; Plata, D. L.; O'Brien, K. P.; Hart, A. J.; Meshot, E. R.; Reddy, C. M.; Gschwend, P. M.; Thompson, C. V. Precursor Gas Chemistry Determines the Crystallinity of Carbon Nanotubes Synthesized at Low Temperature. *Carbon* **2011**, *49*, 804–810.
22. Magrez, A.; Smajda, R.; Seo, J. W.; Horvath, E.; Ribic, P. R.; Andresen, J. C.; Acquaviva, D.; Olariu, A.; Laurenczy, G.; Forro, L. Striking Influence of the Catalyst Support and Its Acid-Base Properties: New Insight into the Growth Mechanism of Carbon Nanotubes. *ACS Nano* **2011**, *5*, 3428–3437.
23. Stine, B. E.; Ouma, D. O.; Divecha, R. R.; Boning, D. S.; Chung, J. E.; Hetherington, D. L.; Harwood, C. R.; Nakagawa, O. S.; Oh, S. Y. Rapid Characterization and Modeling of Pattern-Dependent Variation in Chemical-Mechanical Polishing. *IEEE Trans. Semiconduct. Manufact.* **1998**, *11*, 129–140.
24. Abrokwah, K. O.; Chidambaram, P. R.; Boning, D. S. Pattern Based Prediction for Plasma Etch. *IEEE Trans. Semiconduct. Manufact.* **2007**, *20*, 77–86.
25. Latorre, N.; Romeo, E.; Cazana, F.; Ubieto, T.; Royo, C.; Villacampa, J. J.; Monzon, A. Carbon Nanotube Growth by Catalytic Chemical Vapor Deposition: A Phenomenological Kinetic Model. *J. Phys. Chem. C* **2010**, *114*, 4773–4782.
26. Bedewy, M.; Meshot, E. R.; Reinker, M. J.; Hart, A. J. Population Growth Dynamics of Carbon Nanotubes. *ACS Nano* **2011**, *5*, 8974–8989.
27. Puretzky, A. A.; Geohegan, D. B.; Jesse, S.; Ivanov, I. N.; Eres, G. *In Situ* Measurements and Modeling of Carbon Nanotube Array Growth Kinetics during Chemical Vapor Deposition. *Appl. Phys. A: Mater. Sci. Process.* **2005**, *81*, 223–240.
28. Moseler, M.; Cervantes-Sodi, F.; Hofmann, S.; Csanyi, G.; Ferrari, A. C. Dynamic Catalyst Restructuring during Carbon Nanotube Growth. *ACS Nano* **2010**, *4*, 7587–7595.
29. Wirth, C. T.; Bayer, B. C.; Gamalski, A. D.; Esconjauregui, S.; Weatherup, R. S.; Ducati, C.; Baehtz, C.; Robertson, J.; Hofmann, S. The Phase of Iron Catalyst Nanoparticles during Carbon Nanotube Growth. *Chem. Mater.* **2012**, *24*, 4633–4640.
30. Hofmann, S.; Sharma, R.; Ducati, C.; Du, G.; Mattevi, C.; Cepek, C.; Cantoro, M.; Pisana, S.; Parvez, A.; Cervantes-Sodi, F.; Ferrari, A. C.; Dunin-Borkowski, R.; Lizzit, S.; Petaccia, L.; Goldoni, A.; Robertson, J. *In Situ* Observations of Catalyst Dynamics during Surface-Bound Carbon Nanotube Nucleation. *Nano Lett.* **2007**, *7*, 602–608.
31. Ding, F.; Harutyunyan, A. R.; Yakobson, B. I. Dislocation Theory of Chirality-Controlled Nanotube Growth. *Proc. Natl. Acad. Sci. U.S.A.* **2009**, *106*, 2506–2509.
32. Rao, R.; Liptak, D.; Cherukuri, T.; Yakobson, B. I.; Maruyama, B. *In Situ* Evidence for Chirality-Dependent Growth Rates of Individual Carbon Nanotubes. *Nat. Mater.* **2012**, *11*, 213–216.
33. Geohegan, D. B.; Puretzky, A. A.; Jackson, J. J.; Rouleau, C. M.; Eres, G.; More, K. L. Flux-Dependent Growth Kinetics and Diameter Selectivity in Single-Wall Carbon Nanotube Arrays. *ACS Nano* **2011**, *5*, 8311–8321.
34. Bedewy, M.; Hart, A. J. Mechanical Coupling Limits the Density and Quality of Self-Organized Carbon Nanotube Growth. *Nanoscale* **2013**, *5*, 2928–2937.

35. Hirschfelder, J. O.; Curtiss, C. F.; Bird, R. B. *The Molecular Theory of Gases and Liquids*; Wiley: New York, 1964.
36. Bedewy, M.; Meshot, E. R.; Hart, A. J. Diameter-Dependent Kinetics of Activation and Deactivation in Carbon Nanotube Population Growth. *Carbon* **2012**, *50*, 5106–5116.
37. Bedewy, M.; Meshot, E.; Guo, H.; Verploegen, E.; Lu, W.; Hart, A. Collective Mechanism for the Evolution and Self-Termination of Vertically Aligned Carbon Nanotube Growth. *J. Phys. Chem. C* **2009**, *113*, 20576–20582.
38. Park, S. J.; Schmidt, A. J.; Bedewy, M.; Hart, A. J. Measurement of Carbon Nanotube Microstructure Relative Density by Optical Attenuation and Observation of Size-Dependent Variations. *Phys. Chem. Chem. Phys.* **2013**, *15*, 11511–11519.
39. Moulton, K.; Morrill, N. B.; Konneker, A. M.; Jensen, B. D.; Vanfleet, R. R.; Allred, D. D.; Davis, R. C. Effect of Iron Catalyst Thickness on Vertically Aligned Carbon Nanotube Forest Straightness for CNT-MEMS. *J. Micromech. Microeng.* **2012**, *22*, 055004.
40. Zhong, G. F.; Iwasaki, T.; Robertson, J.; Kawarada, H. Growth Kinetics of 0.5 cm Vertically Aligned Single-Walled Carbon Nanotubes. *J. Phys. Chem. B* **2007**, *111*, 1907–1910.
41. Zhu, L. B.; Hess, D. W.; Wong, C. P. Monitoring Carbon Nanotube Growth by Formation of Nanotube Stacks and Investigation of the Diffusion-Controlled Kinetics. *J. Phys. Chem. B* **2006**, *110*, 5445–5449.
42. Wirth, C. T.; Zhang, C.; Zhong, G. F.; Hofmann, S.; Robertson, J. Diffusion- and Reaction-Limited Growth of Carbon Nanotube Forests. *ACS Nano* **2009**, *3*, 3560–3566.
43. Zhang, G. Y.; Mann, D.; Zhang, L.; Javey, A.; Li, Y. M.; Yenilmez, E.; Wang, Q.; McVittie, J. P.; Nishi, Y.; Gibbons, J.; Dai, H. J. Ultra-High-Yield Growth of Vertical Single-Walled Carbon Nanotubes: Hidden Roles of Hydrogen and Oxygen. *Proc. Natl. Acad. Sci. U.S.A.* **2005**, *102*, 16141–16145.
44. Magrez, A.; Seo, J. W.; Kuznetsov, V. L.; Forro, L. Evidence of an Equimolar C_2H_2-CO_2 Reaction in the Synthesis of Carbon Nanotubes. *Angew. Chem., Int. Ed.* **2007**, *46*, 441–444.
45. Nasibulin, A. G.; Brown, D. P.; Queipo, P.; Gonzalez, D.; Jiang, H.; Kauppinen, E. I. An Essential Role of CO_2 and H_2O during Single-Walled CNT Synthesis from Carbon Monoxide. *Chem. Phys. Lett.* **2006**, *417*, 179–184.
46. Liu, K.; Liu, P.; Jiang, K.; Fan, S. S. Effect of Carbon Deposits on the Reactor Wall during the Growth of Multi-Walled Carbon Nanotube Arrays. *Carbon* **2007**, *45*, 2379–2387.